

Synaptic plasticity shapes top-down modulation of cortical circuits with multiple interneuron types

Abstract

1 Introduction

2 Results

3 Training of assemblies in cortical circuits with multiple interneuron subtypes

4 *Needs details: What brain region was modeled? Why were these plasticity mechanisms introduced?

5 We set out to investigate the emergence and maintenance of neuronal assemblies in large scale
6 spiking networks with an excitatory neuron population and three different types of inhibitory interneurons
7 (PV, SST and VIP neurons, Fig. 1A). These populations interact with each other and, crucially, constitute
8 multiple sources of inhibitory control over excitatory neurons. In agreement with experimental findings
9 (REF), we considered two scenarios where excitatory to excitatory and inhibitory to excitatory synaptic
10 strengths are modified by synaptic plasticity. In the first scenario, inhibitory synapses from PV and SST
11 onto excitatory neurons follow an inhibitory STDP rule, which homeostatically regulated excitatory firing
12 rates by ensuring that they achieve a target level of firing (Vogels et al., 2011). In the second scenario,
13 only synapses from PV onto excitatory neurons are plastic while SST synapses are static. In addition,
14 we also included heterosynaptic competition where the neurons total synaptic strengths incoming into
15 a neuron are maintained at a constant level, to prevent the weight dynamics rowing out of bound.

16 In the baseline state, all excitatory neurons in the network received the same input, resulting in
17 asynchronous irregular spiking (Fig. 1B), similar to the spiking in balanced networks with a single in-
18 hibitory interneuron population (Brunel, 2000). To form neuronal assemblies via synaptic plasticity, we
19 assumed that subsets of neurons which share stimulus preference, would be activated together. For
20 example, in the primary visual cortex, neurons that are selective to the same orientation, become more
21 strongly connected shortly after eye opening (Ko et al.). To model this, we co-activated non-overlapping
22 subgroups of neurons in random order during training with elevated firing rates (Fig. 1E, Methods). Dur-
23 ing training, synapses between excitatory neurons within one subgroup strengthen such that they form
24 neuronal assemblies (Fig. 1C, top left), while synapses between excitatory neurons in different groups
25 become weaker (Fig. 1C, bottom left). These induced differences remain for a long time after the end
26 of training (dashed lines in Fig. 1C). In the first scenario, inhibitory synapses from both PV (Fig. 1C,
27 top right) and SST (Fig. 1C, bottom right) subtypes potentiate during training in responses to these in-
28 creases in excitatory firing. After training, they depress, but still remains well above the baseline values
29 to balance the activity-dependent reorganization of excitatory connectivity into assemblies. Similarly, in
30 the second scenario, the plasticity of PV to excitatory neurons alone is sufficient to stabilize training and
31 promote the formation of neuronal assemblies (Supplementary Fig. S1).

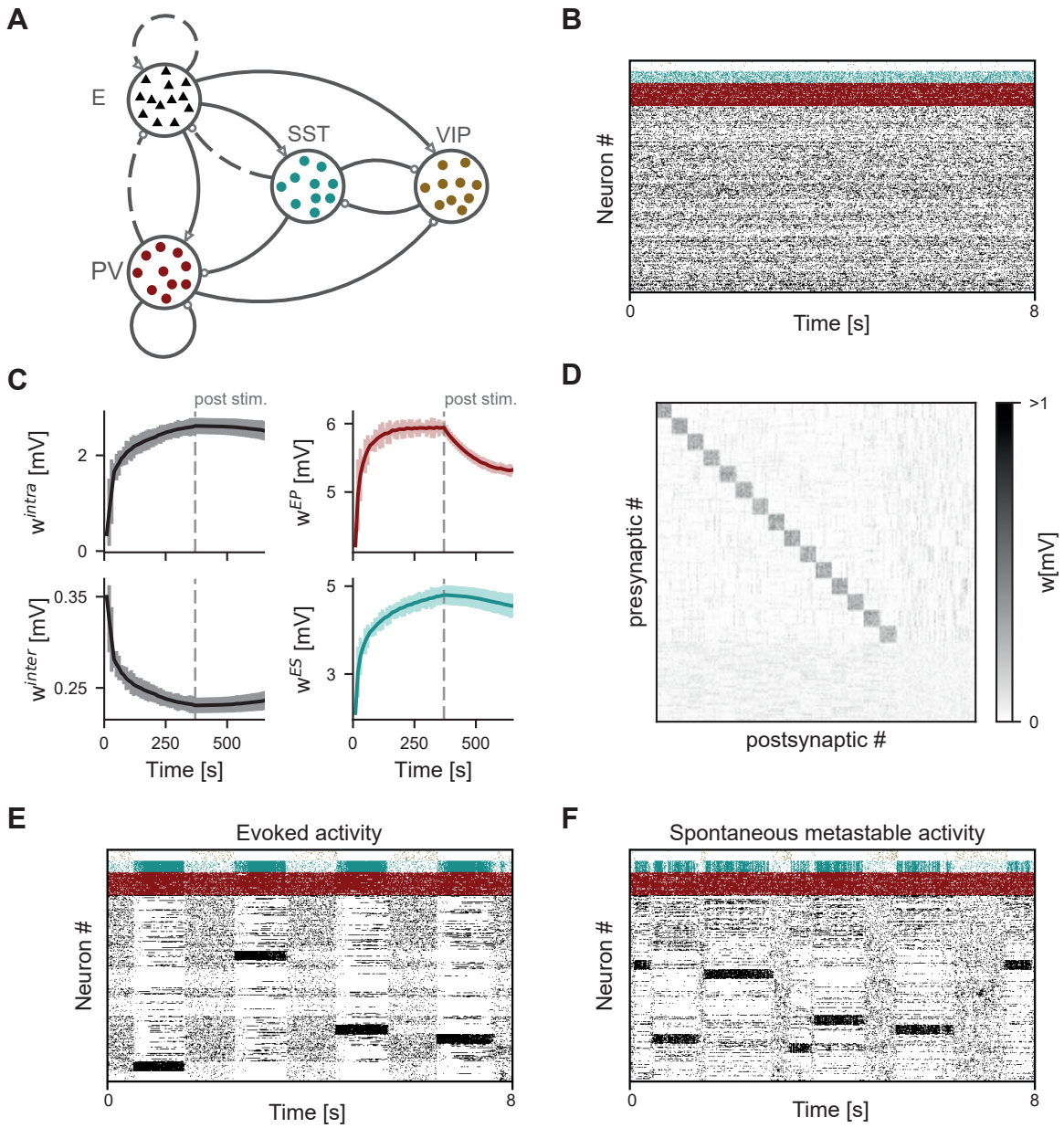


Figure 1: Stable, spontaneously reactivating assemblies emerge in a cortical circuit model with multiple inhibitory interneuron subtypes. (A) Schematic of the model with excitatory neurons (E), parvalbumin-positive (PV), somatostatin-positive (SST), and vasointestinal peptide-positive (VIP) interneurons. Dashed lines denote connections that are plastic during training, solid lines denote connections that have constant values. **(B)** Spike raster plot showing asynchronous-irregular firing in the network before training. **(C)** Development of weights during training and spontaneous activity (end of training at dashed line) with SST and PV plasticity. Mean weights between neurons within the same assembly (w^{intra} , upper left), and between neurons in different assemblies (w^{inter} , lower left). Inhibitory weights from PV to excitatory assembly neurons (w^{EP} , upper right, absolute values) and from SST to excitatory assembly neurons (w^{ES} , lower right, absolute values). Shaded areas denote standard deviation. **(D)** Connection strengths between excitatory neurons after training, sorted by assembly membership. **(E)** Spike raster plot showing evoked structured spiking activity during training. **(F)** Spike raster plot showing spontaneous metastable spiking activity after training.

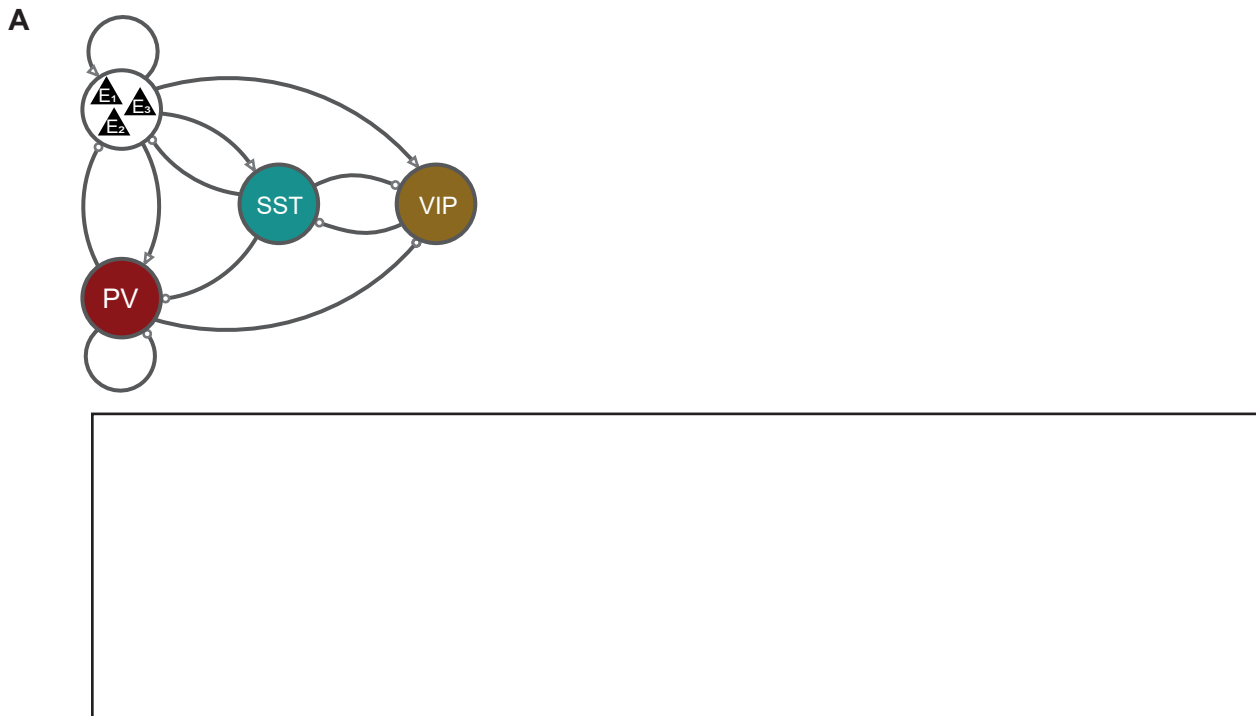


Figure 2: MFT-proposal: Mean-field analysis of a clustered network with multiple interneuron subtypes reveals the emergence of an attractor landscape. (A) Schematic of the mean-field population model.

When excitatory neurons are sorted by stimulus preference, the increased connection strength of neurons within assemblies is visible as a characteristic block-diagonal structure (Fig. 1D). Similar to networks with only one inhibitory interneuron population, we found that these assemblies show spontaneously reverberating patterns of activity called metastable states (La Camera et al., 2019) which stabilize excitatory connectivity in the absence of structured input (Litwin-Kumar and Doiron, 2014) (Fig. 1F). Importantly, these patterns of spontaneous activity resemble those of evoked activity, a feature frequently observed experimentally (La Camera et al., 2019; Miller et al., 2014).

The emergence of an attractor landscape explains spontaneous activity in the spiking network

(Note: Proposal to put here mean-field theory for clustered network with multiple interneuron subtypes for explaining the basics of the metastable activity)

Top-down modulation of VIP has opposite effects on the dynamics for different interneuronal circuitry

Needs details: What is the significance of top-down inputs? Where do they come from?

Top-down inputs targeting excitatory or inhibitory neurons alter the temporal dynamics of metastable activity in spiking neural networks with one excitatory and one inhibitory population (Mazzucato et al., 2019; Wyrick and Mazzucato, 2021). To test how top-down inputs alter metastable activity in our network with multiple interneuron subtypes, we turned off plasticity and then globally increased the input

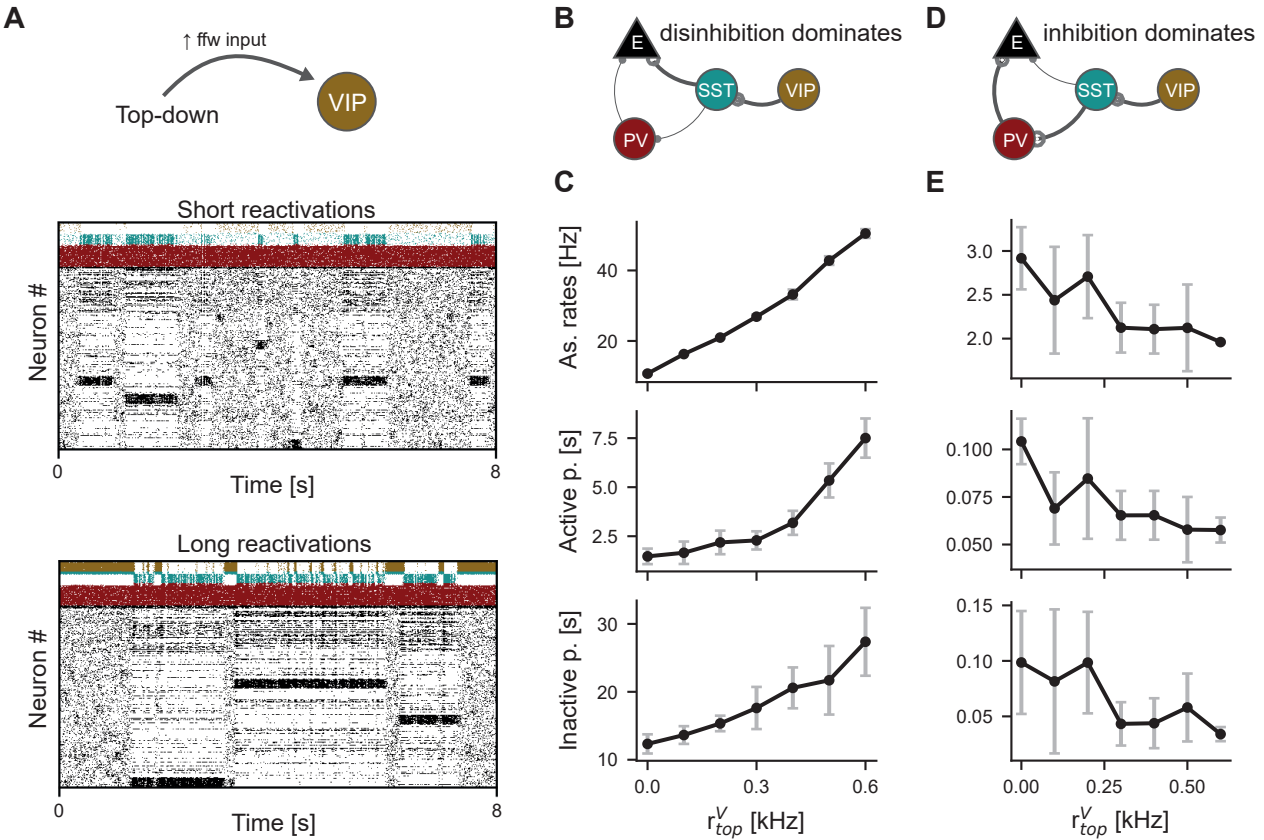


Figure 3: Opposite effects of VIP-modulation on spontaneous activity for different interneuronal circuitry.

(A) Top-down inputs alter the temporal dynamics of metastable activity. I would show the whole circuit again. Short reactivations and faster dynamics, top spike raster plot. Long reactivations and slower dynamics, bottom spike raster plot. (B) When SST-projections to excitatory neurons are strong, VIP-modulation effectively disinhibits excitatory neurons. I would show an arrow into VIP here and in C. Also, might want to color the pathway lines, not thicken them (could be confused with potentiation). (C) Effects of increasing modulation of VIP-interneurons with dominant disinhibition on mean rate of active assemblies (top), mean duration of active periods (middle), and mean duration of inactive periods (bottom). Error bars denote standard error of the mean for five simulations of 200 s each. (D) When SST-projections to excitatory neurons are weak, VIP-modulation effectively inhibits excitatory neurons. (E) Same as (C) for effective inhibition of excitatory neurons by VIP-modulation.

to VIP neurons which are a prominent target of top-down signals (Batista-Brito et al., 2018). Elaborate on this, VIP as the target of top-down modulation.

We found that top-down inputs targeting VIP neurons alter the temporal dynamics of metastable activity in the network with multiple interneurons (Fig. 3A). However, the direction of this modulation is highly dependent on the underlying network connectivity. In the first scenario with plasticity from both SST and PV to excitatory neurons during training, both SST and PV synapses to excitatory neurons strongly potentiate (Fig. 1). Thus, VIP activation inhibits SST neurons which in turn leads to SST-mediated disinhibition of excitatory neurons (Fig. 3B). This leads to gradual increases in the firing of reverberating assemblies and their activation and inactivation times as a function of top-down input (Fig. 3C). We call this the disinhibition dominated network. In the second scenario only with plasticity from PV to excitatory neurons during training, only PV synapses potentiate. Upon activating VIP neurons, excitatory neurons are inhibited through the disinhibition of PV (Fig. 3D). With increasing top-

62 down input, assembly reactivation rates as well as activation and inactivation times decrease (Fig. 3D),
63 leading to an overall acceleration of the temporal dynamics of metastable activity, which resembles
64 metastable dynamics in the rat gustatory cortex during general expectation (Mazzucato et al., 2019).
65 We call this the inhibition dominated network.

66 Taken together, these results show that VIP-mediated top-down signals can alter the temporal dy-
67 namics of metastable activity in a model of the sensory cortical circuit that includes multiple inhibitory
68 interneuron subtypes. Crucially, our results highlight the role of the interactions between these multiple
69 subtypes of interneurons in the network in shaping the effects of top-down inputs.

70 **Network connectivity determines the effects of direct top-down modulation of excitatory 71 neurons**

72 In addition to VIP neurons, pyramidal excitatory neurons in the neocortex are also prominent targets of
73 top-down inputs (Doron et al., 2020). We therefore also studied the effects of modulations directly tar-
74 geting excitatory neurons in the network. Building on previous work in networks with only one inhibitory
75 interneuron population, we targeted excitatory neurons in two different ways: (1) by increasing the
76 mean input and (2) by changing the variance of the inputs across neurons in the excitatory population
77 (Mazzucato et al., 2019; Wyrick and Mazzucato, 2021).

78 In the disinhibition dominated network, increasing the feedforward input to excitatory neurons in-
79 creases the rates of assembly reactivations and slows down the overall temporal dynamics of metastable
80 activity (Fig. 4A). This effect is qualitatively similar to VIP-mediated top-down modulation (Fig. 3C).
81 However, when we increased the input variance, we observed the opposite behavior: temporal dynam-
82 ics of the metastable activity become faster, accompanied by a decrease of assembly reactivation rates
83 (Fig. 4B). This is in contrast to previous work in two-population excitatory-inhibitory networks where both
84 kinds of top-down inputs – increase of variance and increase of mean – elicited the same network re-
85 sponds, namely an acceleration of network dynamics (Wyrick and Mazzucato, 2021). Interestingly, this
86 bidirectionality is specific to the network with dominant disinhibition and is broken in the inhibition domi-
87 nated network, where both perturbations lead to a slow-down of the network dynamics (Fig. 4C and D).
88 This suggests an advantage of operating in a regime where the disinhibitory pathway dominates the
89 interaction between VIP and excitatory neurons, as the circuit interactions diversify the realm of net-
90 work responses to top-down inputs targeting the excitatory population. In fact, disinhibition of excitatory
91 neurons in response to VIP neuron activation is more prominent than inhibition (Guet-McCreight et al.,
92 2020), and it would be interesting to test experimentally how metastable activity is differently shaped
93 across cortical regions by the same kinds of perturbations.

94 **Top-down inputs modulate the attractor landscape, altering the overall temporal dynam- 95 ics of metastable activity**

96 (Note: Here, proposal to show changes in energy landscape of the MFT)

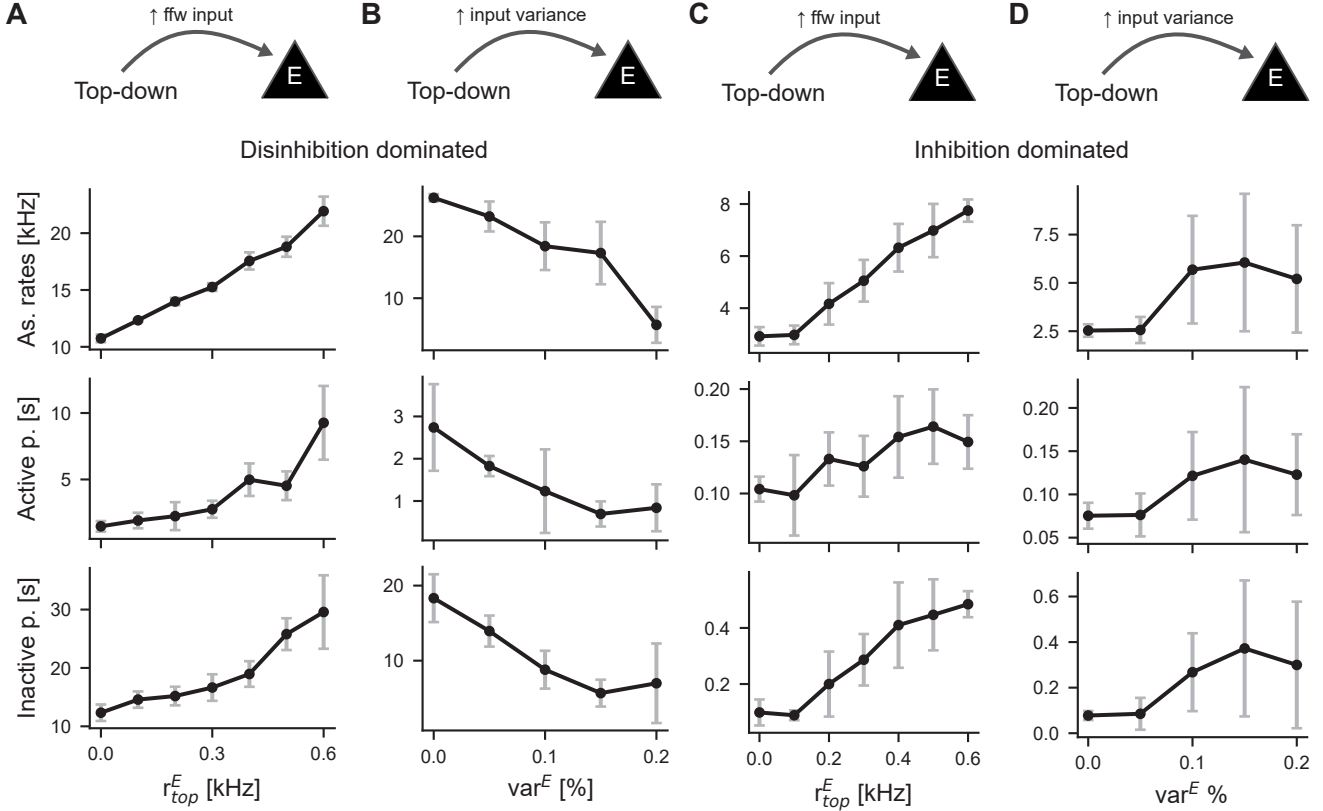


Figure 4: Modulation of mean and of variability of inputs to excitation has different effects depending on the underlying network connectivity. (A) Top-down modulation of excitatory neurons through change of the mean input in the disinhibition dominated network. Effects of increasing mean modulation of excitatory neurons on rates of active assemblies (top), mean duration of active periods (middle), and mean duration of inactive periods (bottom) in the inhibition dominated network. Error bars denote standard error of the mean for five simulations of 200 s each. **(B)** Top-down modulation of excitatory neurons through increasing the input variance across neurons. Measures are the same as in (A). The x-axis is the standard deviation of the normal distribution from which input values are drawn in percent of average input. **(C)** same as (A) for the inhibition dominated network. **(D)** same as (B) for the inhibition dominated network.

97 Discussion

98 Materials and Methods

99 Neuron and network model

100 We modeled a recurrent spiking network of the mouse cortical microcircuit, comprising four populations
 101 of neurons – one excitatory and three inhibitory interneuron populations (Fig. 1A). The network consists
 102 of a total of 4000 excitatory neurons and 1000 inhibitory interneurons (500 PV, 250 SST and 250
 103 VIP). Single neurons were modeled as leaky-integrate-and-fire neurons with the membrane voltage
 104 dynamics:

$$\frac{dV}{dt} = -\frac{V}{\tau_m} + \sum_X I^X. \quad (1)$$

105 The input current for each neuron was defined as the sum over all input sources X, which include
 106 external feedforward excitatory inputs and recurrent synaptic inputs from other neurons in the network
 107 (excitatory, PV, SST and VIP).

108 Upon reaching the spiking threshold V_{thr} , the neuron elicited a spike and the membrane potential was
 109 reset to V_{res} , where it was clamped for an absolute refractory period τ_{abs} .

110 Connections between neurons of different populations were constrained by experimental findings
 111 (Jiang et al., 2015; Pfeffer et al., 2013). Excitatory neurons target all other neuron populations and
 112 are inhibited by PV and SST neurons. VIP neurons inhibit SST neurons which in turn inhibit PV and
 113 VIP neurons. PV neurons target other PV neurons and VIP neurons. For the interacting neuron types,
 114 connections were chosen randomly with probability 0.1, with autapses being removed later.

115 We used current-based synapses. Synaptic currents decayed exponentially with time constant τ^X .
 116 For every presynaptic spike, the synaptic current was updated according to the weight w_{ij} for a synapse
 117 from presynaptic neuron j to postsynaptic neuron i :

Table 1: Neuron and network parameters.

Paramter	Description	Value
V_{thr}	Threshold potential	10 mV
V_{res}	Reset potential	0 mV
τ_m	Membrane time constant	20 ms
τ_{abs}	Absolute refractory period	1 ms
τ^E	E synaptic time constant	3 ms
τ^P	PV synaptic time constant	4 ms
τ^S	SST synaptic time constant	5 ms
τ^V	VIP synaptic time constant	5 ms
$w^E(0)$	Initial E to E synaptic weight	0.35 mV
w_{min}^{EE}	Min. E to E synaptic weight	$0.1 \cdot w^{EE}(0)$
w_{max}^{EE}	Max. E to E synaptic weight	$10 \cdot w^{EE}(0) / 20 \cdot w^{EE}(0)^*$
w^{PE}	E to PV synaptic weight	$4 \cdot w^{EE}(0)$
w^{SE}	E to SST synaptic weight	$0.2 \cdot w^{EE}(0)$
w^{VE}	E to VIP synaptic weight	$0.2 \cdot w^{EE}(0)$
$w^{EP}(0)$	Initial PV to E synaptic weight	$12 \cdot w^{EE}(0)$
w_{min}^{EP}	Min. PV to E synaptic weight	$w^{EP}(0)$
w_{max}^{EP}	Max. PV to E synaptic weight	$30 \cdot w^{EE}(0)$
w^{PP}	PV to PV synaptic weight	$9 \cdot w^{EE}(0)$
w^{VP}	PV to VIP synaptic weight	$0.2 \cdot w^{EE}(0)$
$w^{ES}(0)$	Initial SST to E synaptic weight	$4 \cdot w^{EE}(0)$
w_{min}^{ES}	Min. SST to E synaptic weight	$w^{ES}(0)$
w_{max}^{ES}	Max. SST to E synaptic weight	$10 \cdot w^{EE}(0)$
w^{PS}	SST to PV synaptic weight	$4 \cdot w^{EE}(0)$
w^{VS}	SST to VIP synaptic weight	$6 \cdot w^{EE}(0)$
w^{SV}	VIP to SST synaptic weight	$1.5 \cdot w^{EE}(0)$
w^{EF}	FFW to E synaptic weight	$w^{EE}(0)$
w^{PF}	FFW to PV synaptic weight	$0.7 \cdot w^{EE}(0)$
w^{SF}	FFW to SST synaptic weight	$0.25 \cdot w^{EE}(0)$
w^{VF}	FFW to VIP synaptic weight	$0.27 \cdot w^{EE}(0)$

$$\frac{dI_i^X}{dt} = -\frac{I_i^X}{\tau_i^X} \quad \text{if } t = t^{pre}, I_i^X \rightarrow I_i^X + \frac{w_{ij}}{\tau_i^X} \quad (2)$$

118 After an equilibration phase of 100 ms, designated synapse types changed weights according to dif-
 119 ferent plasticity rules. We studied two networks. In the first one, excitatory synapses onto excitatory
 120 neurons and both SST and PV synapses onto excitatory neurons were plastic. In the second one, SST
 121 synapses were static (differing parameters marked with an asterisk in table 1 and 2 and the text).

122 Excitatory plasticity

123 Synapses between excitatory neurons were plastic according to a triplet STDP rule (Pfister and Gerst-
 124 ner, 2006) which allows for bidirectional strengthening of connections as observed in neuronal assem-
 125 blies (Cossell et al., 2015; Ko et al., 2013; Montangie et al., 2020). To set the contribution of a spike
 126 to the update of a synaptic weight, spike timing differences were traced via four exponentially decaying
 127 spike detectors with time constants τ_+ , τ_x , τ_- , τ_y . The spike detectors were updated by 1 when a pre-
 128 (r) or postsynaptic (o) spike occurred.

$$\frac{dr_1(t)}{dt} = -\frac{r_1(t)}{\tau_+} \quad \text{if } t = t^{pre}, r_1(t) \rightarrow r_1(t) + 1 \quad (3)$$

$$\frac{dr_2(t)}{dt} = -\frac{r_2(t)}{\tau_x} \quad \text{if } t = t^{pre}, r_2(t) \rightarrow r_2(t) + 1 \quad (4)$$

$$\frac{do_1(t)}{dt} = -\frac{o_1(t)}{\tau_-} \quad \text{if } t = t^{post}, o_1(t) \rightarrow o_1(t) + 1 \quad (5)$$

$$\frac{do_2(t)}{dt} = -\frac{o_2(t)}{\tau_y} \quad \text{if } t = t^{post}, o_2(t) \rightarrow o_2(t) + 1. \quad (6)$$

129 The traces scale the update of the excitatory synaptic weights upon a pre- or postsynaptic spike within

Table 2: Parameters for synaptic plasticity.

Paramter	Description	Value
A_2^+	Pair potentiation amplitude	$7.5 \cdot 10^{-10}$ mV
A_2^-	Pair depression amplitude	$7 \cdot 10^{-3}$ mV
A_3^+	Triplet potentiation amplitude	$9.3 \cdot 10^{-3}$ mV
A_3^-	Triplet depression amplitude	$2.3 \cdot 10^{-4}$ mV
η	iSTDP learning rate	0.01 mV / 0.1 mV*
τ_+	Time constant for detector r_1	16.8 mV
τ_x	Time constant for detector r_1	101.0 mV
τ_-	Time constant for detector o_1	33.7 mV
τ_y	Time constant for detector o_2	125 mV
τ_{iSTDP}	Time constant for iSTDP	20 mV
ρ_0	Target firing rate	3 Hz / 2.5 Hz*
τ_{norm}	Time constant for normalisation	20 ms

130 the range defined (lower and upper bounds, see Tab. 1)

$$w(t) \rightarrow w(t) - o_1(t)[A_2^- + A_3^- r_2(t - \epsilon)] \quad \text{if } t = t^{pre} \quad (7)$$

$$w(t) \rightarrow w(t) + r_1(t)[A_2^+ + A_3^+ o_2(t - \epsilon)] \quad \text{if } t = t^{post}. \quad (8)$$

131 The amplitudes A_2^+ , A_2^- , A_3^+ , A_3^- determine the amount of synaptic potentiation (+) or depression
 132 (-) resulting from pairs ('2') and triplets ('3') of spikes. Pre-post pairs and 1-pre-2-post triplets induce
 133 potentiation, post-pre pairs and 2-pre-1-post triplets lead to depression of the respective synapses.
 134 The parameter ϵ is a small positive number that ensures that synaptic weights are updated before the
 135 updates of the pre- and postsynaptic detectors occur.

136 To avoid saturating synaptic weights, we included heterosynaptic competition between excitatory
 137 synapses that target the same postsynaptic excitatory neuron. Every 20 ms, synaptic weights were
 138 subtractively normalized such that the total incoming synaptic weights were approximately constant for
 139 each neuron:

$$w_{ij}^{EE}(t) \rightarrow w_{ij}^{EE}(t) - \frac{\sum_j (w_{ij}^{EE}(t) - w_{ij}^{EE}(0))}{N_i^E} \quad (9)$$

140 where N_i^E is the number of all excitatory synapses that target excitatory neuron i .

141 Inhibitory plasticity

142 Inhibitory synapses from PV, and if plastic, from SST neurons onto excitatory neurons were governed
 143 by a pair-based inhibitory STDP rule which homeostatically regulates excitatory firing (Vogels et al.,,
 144 2011). Analogous to the triplet STDP, spike detectors were modeled as decaying exponentials, with
 145 time constant τ_{iSTDP} both for the inhibitory (x_{pre}) and excitatory (x_{post}) trace, and updated by 1 when a
 146 respective spike occurred:

$$\frac{x_{pre}(t)}{dt} = -\frac{x_{pre}(t)}{\tau_{iSTDP}} \quad \text{if } t = t^{pre}, \quad x_{pre}(t) \rightarrow x_{pre}(t) + 1 \quad (10)$$

$$\frac{x_{post}(t)}{dt} = -\frac{x_{post}(t)}{\tau_{iSTDP}} \quad \text{if } t = t^{post}, \quad x_{post}(t) \rightarrow x_{post}(t) + 1 \quad (11)$$

147 Upon a pre- or postsynaptic spike, inhibitory synapse weights were updated within the lower and upper
 148 bounds as:

$$w(t) \rightarrow w(t) + \eta(x_{post}(t) - 2\rho_0\tau_{iSTDP}) \quad \text{if } t = t^{pre} \quad (12)$$

$$w(t) \rightarrow w(t) + \eta x_{pre}(t) \quad \text{if } t = t^{post} \quad (13)$$

149 where the parameter η , referred to as the learning rate, scales the overall amount of long-term plas-
 150 ticity elicited by spike pairs, similar to the amplitudes in the triplet STDP. The parameter ρ_0 denotes a
 151 target set-point for the firing rate of the postsynaptic excitatory neuron. A presynaptic spike that is not
 152 paired with a postsynaptic spike leads to depression of the synaptic weight by $\eta \cdot 2\rho_0\tau_{iSTDP}$. When a
 153 presynaptic spike and a postsynaptic spike occur in close temporal proximity, the extent of potentiation

154 is determined by the time difference between the pre- and postsynaptic spike.

155 **Stimulation protocol for assembly formation**

156 To induce the formation of neuronal assemblies, excitatory neurons were partitioned into an unclustered
157 background (1000 neurons) and a clustered (3000 neurons) group. Within the clustered group, neurons
158 were further divided into 15 subgroups containing 200 neurons each. All neurons received a constant
159 feedforward input in the form of spike trains that follow Poisson statistics with a rate of 5 kHz. After
160 the pre-training, all 15 subgroups consecutively and randomly received additional input for one second,
161 followed by a one second break. Stimulation of the groups was implemented as selective increase of
162 the rates of the feedforward input Poisson processes by 100% / 200%*. This stimulation protocol was
163 repeated for $N_{trials} = 12$ (360 s).

164 **Top-down modulation**

165 For studying top-down modulation, we inactivated both excitatory and inhibitory plasticity 130 seconds
166 after training. Inactivation of inhibitory STDP was necessary because the STDP rule prevents lasting
167 changes in excitatory firing rates (Vogels et al., 2011) which we wanted to include to study the effects of
168 top-down modulation. Inactivation of the plasticity between excitatory neurons was necessary because
169 the network with excitatory plasticity is unstable without firing homeostasis (Zenke et al., 2015). Excita-
170 tory or VIP neurons received top-down inputs in two ways. First, all neurons of the targeted population
171 experienced higher feedforward drive by increasing the mean rate of the Poisson spike trains that each
172 neuron received as background input. Alternatively, the input variance across neurons was altered
173 (Mazzucato et al., 2019). For the modulation of variance across neurons, feedforward input synaptic
174 weights were drawn from a normal distribution with the average synaptic weight fixed to the initial level
175 and a defined standard deviation, with a higher standard deviation corresponding to stronger top-down
176 input (Table 1).

177 **Analysis of metastable activity**

178 In order to characterize metastable activity in the spiking neural network, we determined active peri-
179 ods, the average firing rate during active periods and the inactive periods of each excitatory neuron
180 subgroup. For each stimulation value (feedforward input or variance across neurons), we computed the
181 average firing rates of excitatory neuron subgroups, binning spike counts in time bins of $t_{bin} = 50$ ms
182 / $t_{bin} = 5$ ms* for a total duration of 200 s. Rates were smoothed over ten / two* bins with a Gaus-
183 sian window with a standard deviation of 2 Hz. We computed a dynamic threshold, set to the overall
184 average firing rate of the unclustered background population for each simulation with varying input
185 strengths. Whenever an excitatory neuron subgroup exceeded this threshold, it was classified as active
186 and otherwise, as inactive.

187 **Mean field theory**

188 **Simulation details**

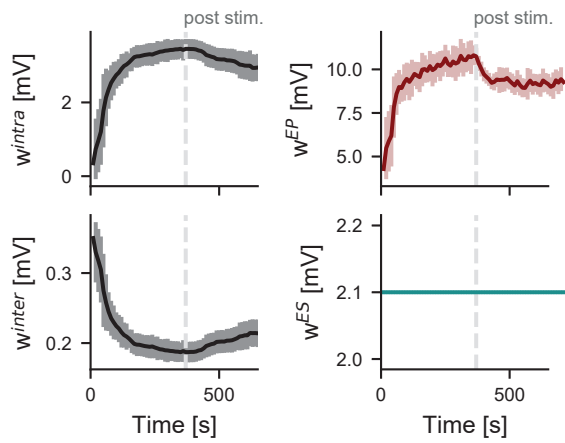
189 Numerical simulations of the spiking network were performed using custom code in Julia 1.6. Differential
190 equations were discretized using the forward Euler algorithm with a timestep of 0.1 ms. Analysis of the
191 spiking neural network data was performed using Python 3.9. Visualization and analysis of the MFT
192 was performed using Matlab (version...). The code for the implementation of the spiking neural network
193 and the MFT will be made available upon publication.

194 **References**

- 195 Batista-Brito, R., Zagha, E., Ratliff, J. M., and Vinck, M. (2018). Modulation of cortical circuits by top-
196 down processing and arousal state in health and disease. *Curr Opin Neurobiol*, 52:172–181.
- 197 Brunel, N. (2000). Dynamics of sparsely connected networks of excitatory and inhibitory spiking neu-
198 rons. *J Comput Neurosci*, 8:183–208.
- 199 Cossell, L., Iacaruso, M. F., Muir, D. R., Houlton, R., Sader, E. N., Ko, H., Hofer, S. B., and Mrsic-Flogel,
200 T. D. (2015). Functional organization of excitatory synaptic strength in primary visual cortex. *Nature*,
201 518:399–403.
- 202 Doron, G., Shin, J. N., Takahashi, N., Drüke, M., Bocklisch, C., Skenderi, S., Mont, L. D., Toumazou,
203 M., Ledderose, J., Brecht, M., Naud, R., and Larkum, M. E. (2020). Perirhinal input to neocortical
204 layer 1 controls learning. *Science (New York, N.Y.)*, 370.
- 205 Guet-McCreight, A., Skinner, F. K., and Topolnik, L. (2020). Common principles in functional organiza-
206 tion of vip/calretinin cell-driven disinhibitory circuits across cortical areas. *Frontiers in Neural Circuits*,
207 14.
- 208 Jiang, X., Shen, S., Cadwell, C. R., Berens, P., Sinz, F., Ecker, A. S., Patel, S., and Tolias, A. S. (2015).
209 Principles of connectivity among morphologically defined cell types in adult neocortex. *Science*,
210 350:aac9462.
- 211 Ko, H., Cossell, L., Baragli, C., Antolik, J., Clopath, C., Hofer, S. B., and Mrsic-Flogel, T. D. (2013). The
212 emergence of functional microcircuits in visual cortex. *Nature*, 496:96–100.
- 213 La Camera, G., Fontanini, A., and Mazzucato, L. (2019). Cortical computations via metastable activity.
214 *Curr Opin Neurobiol*, 58:37–45.
- 215 Litwin-Kumar, A. and Doiron, B. (2014). Formation and maintenance of neuronal assemblies through
216 synaptic plasticity. *Nat Commun*, 5:5319.
- 217 Mazzucato, L., La Camera, G., and Fontanini, A. (2019). Expectation-induced modulation of metastable
218 activity underlies faster coding of sensory stimuli. *Nat Neurosci*, 22:787–796.

- 219 Miller, J.-e. K., Ayzenshtat, I., Carrillo-Reid, L., and Yuste, R. (2014). Visual stimuli recruit intrinsically
220 generated cortical ensembles. *Proc Natl Acad Sci USA*, 111:E4053–E4061.
- 221 Montangie, L., Miehl, C., and Gjorgjieva, J. (2020). Autonomous emergence of connectivity assemblies
222 via spike triplet interactions. *PLoS Comput Biol*, 16.
- 223 Pfeffer, C. K., Xue, M., He, M., Huang, Z. J., and Scanziani, M. (2013). Inhibition of inhibition in visual
224 cortex: the logic of connections between molecularly distinct interneurons. *Nat Neurosci*, 16:1068–
225 1076.
- 226 Pfister, J.-P. and Gerstner, W. (2006). Triplets in a model of spike timing-dependent plasticity. *J Neurosci*,
227 26:9673–9682.
- 228 Vogels, T. P., Sprekeler, H., Zenke, F., Clopath, C., and Gerstner, W. (2011). Inhibitory plasticity balances
229 excitation and inhibition in sensory pathways and memory networks. *Science*, 334:1569–1573.
- 230 Wu, Y. K., Hengen, K. B., Turrigiano, G. G., and Gjorgjieva, J. (2020). Homeostatic mechanisms regulate
231 distinct aspects of cortical circuit dynamics. *Proc Natl Acad Sci USA*, 117:24514–24525.
- 232 Wyrick, D. and Mazzucato, L. (2021). State-dependent regulation of cortical processing speed via gain
233 modulation. *J Neurosci*, 41:3988–4005.
- 234 Zenke, F., Agnes, E. J., and Gerstner, W. (2015). Diverse synaptic plasticity mechanisms orchestrated
235 to form and retrieve memories in spiking neural networks. *Nat Commun*, 6:6922.

²³⁶ **Supplementary figures**



Supplementary Figure S1: Assembly formation in the network with static SST synapses. Development of weights during training and spontaneous activity (end of training at dashed line) with SST and PV plasticity. Mean weights between neurons within the same assembly (w^{intra} , upper left), and between neurons in different assemblies (w^{inter} , lower left). Inhibitory weights from PV to excitatory assembly neurons (w^{EP} , upper right, absolute values) and from SST to excitatory assembly neurons (w^{ES} , lower right, absolute values). Shaded areas denote standard deviation.